Original

Chen, R.; Maawad, E.; Knapp, M.; Ren, S.; Beran, P.; Witter, R.;
Hempelmann, R.:

Lithiation-driven structural transition of VO2F into disordered rock-salt LixVO2F

In: RSC Advances (2016) Royal Society of Chemistry

DOI: 10.1039/C6RA14276A

RSC Advances

PAPER

View Article Online
View Journal | View Issue

Cite this: *RSC Adv.*, 2016, **6**, 65112

Lithiation-driven structural transition of VO_2F into disordered rock-salt Li_xVO_2F

Ruiyong Chen,*[a] Emad Maawad,[b] Michael Knapp,[c] Shuhua Ren,[d] Přemysl Beran,[e] Raiker Witter[f] and Rolf Hempelmann[a]

Received 1st June 2016
Accepted 2nd July 2016

DOI: 10.1039/c6ra14276a

www.rsc.org/advances

We synthesize a new vanadium oxyfluoride VO_2F (rhombohedral, $R\bar{3}c$) through a simple one-step ball-milling route and demonstrate its promising lithium storage properties with a high theoretical capacity of 526 mA h g^{-1}. Similar to V_2O_5, VO_2F transfers into an active disordered rock-salt ($Fm\bar{3}m$) phase after initial cycling against the lithium anode, as confirmed by diffraction and spectroscopic experiments. The newly formed nanosized Li_xVO_2F remains its crystal structure over further cycling between 4.1 and 1.3 V. A high capacity of 350 mA h g^{-1} at 2.5 V was observed at 25 °C and 50 mA g^{-1}. Furthermore, superior performance was observed for VO_2F in comparison with a commercial crystalline V_2O_5, in terms of discharge voltage, voltage hysteresis and reversible capacity.

1. Introduction

High-performance intercalation cathode materials for rechargeable Li-ion batteries are of technical importance.[1–5] Great efforts are devoted to the search of new electrode materials with extended lithium storage capacity. Vanadium is abundant in the crust of the earth. Owing to the multiple oxidation states of vanadium and the varied crystal structure of vanadium oxides and vanadates, vanadium-based electrodes have been widely investigated as alternatives with increased energy densities.[6] Among them, orthorhombic V_2O_5 attracts tremendous attention as cathode materials for accommodating guest cations such as Li^+ ions as well as Mg^{2+} and Al^{3+}.[6–9] It is well recognized that V_2O_5 transforms into several $Li_xV_2O_5$ phases depending on the content of Li^+ intercalated.[10,11] The theoretical capacities of V_2O_5 for two and three lithium intercalation are 294 and 442 mA h g^{-1}, respectively, which are larger than that for classic cathode materials such as $LiFePO_4$ (170 mA h g^{-1}) and $LiCoO_2$ (140 mA h g^{-1}). Intercalation of the third lithium into V_2O_5 occurs at a voltage below 1.9 V, which leads to an irreversible phase transition into disordered rock-salt (ω-$Li_xV_2O_5$, $Fm\bar{3}m$).[11] Lithiation induced structural transition to disordered rock-salt has been observed for other materials, such as Li_2MoO_4,[12] $LiVO_3$ (ref. 13) and $Li_{1.211}Mo_{0.467}Cr_{0.3}O_2$.[14] Disordered rock-salt was also found as intermediate phase during the lithiation reactions of FeOF,[15] Li- and Mn-rich layered materials[16] and spinels.[17] Recent progress in surveying new cathode materials has demonstrated that disordered rock-salt structure is suitable to access high capacity with superior Li^+ chemical diffusion and rigid host framework.[14,18–20]

Variation and modification of V_2O_5 have led to new opportunities to optimize the electrochemical properties. Interestingly, the characteristic lithiation plateau for crystalline orthorhombic V_2O_5 was not observed for amorphous V_2O_5,[21,22] graphene sheets and carbon nanotubes modified V_2O_5 (ref. 23 and 24) and hydrated V_2O_5.[25,26] Meanwhile, enhanced cycling stability and reversible capacity have been achieved. A direct modification of the anion sublattice through fluorine incorporation/substitution in electrode materials has been proven to be an effective strategy to modify and optimize electrochemical performance.[20,27–31] Fluorinated materials are generally synthesized through solution routes using highly toxic and corrosive fluorine-containing acids,[32–34] or by a direct fluorination under reactive conditions of F_2 gas at high temperature.[35] So far, various coordination polymers containing vanadium oxyfluoride matrix have been synthesized and structurally determined.[36,37] However, the existence of inorganic vanadium oxyfluorides is rather rare. VOF_3 is the only commercially available material, which is extremely sensitive to air and moisture and easy to decompose through hydrolysis. In an earlier work,[38] an orange-yellow powder VO_2F was identified by reaction of VOF_3 with $Me_3SiOSiMe_3$ in acetonitrile under an inert atmosphere. However, the structure and applications of VO_2F were unexplored over decades. Recently, VO_2F solid powders have been synthesized under extreme reaction

[a]Joint Electrochemistry Lab, KIST Europe/Saarland University, 66123 Saarbrücken, Germany. E-mail: r.chen@kist-europe.de; ruiyong.chen@uni-saarland.de
[b]Institute of Materials Research, Helmholtz-Zentrum Geesthacht, 22607 Hamburg, Germany
[c]Institute for Applied Materials, Karlsruhe Institute of Technology, 76021 Karlsruhe, Germany
[d]Institute of Nanotechnology, Karlsruhe Institute of Technology, 76021 Karlsruhe, Germany
[e]Nuclear Physics Institute, Academy of Sciences of the Czech Republic, 25068 Řež near Prague, Czech Republic
[f]Technomedicum, Tallinn University of Technology, 19086 Tallinn, Estonia

conditions of high pressure and high temperature (4 GPa and 800 °C).[39] A topotactic intercalation reaction with 0.42 Li^+ has been observed.[39] The structural transition mechanisms remained unclear, regarding to the change in voltage profiles when cycling at a broad voltage range.

Herein, we synthesize rhombohedral VO_2F ($R\bar{3}c$) by a more facile ball-milling process and study the electrochemically driven structural change as cathode material for lithium batteries. The theoretical capacity of VO_2F is 526 mA h g^{-1} based on the assumed intercalation reaction:

$$VO_2F + xLi^+ + xe^- \leftrightarrow Li_xVO_2F \quad (1)$$

supposing that $x = 2$, which is higher than that for $3Li^+$ intercalation of V_2O_5 (442 mA h g^{-1}). Interestingly, similar to orthorhombic V_2O_5, structural phase transitions into disordered rock-salt was observed for VO_2F through the above-mentioned electrochemical lithiation reaction, as confirmed by synchrotron X-ray diffraction, neutron diffraction and *in situ* synchrotron X-ray absorption spectroscopy. Moreover, the cycled VO_2F is isostructural with a previously reported Li_2VO_2F.[20] A comparative investigation among the VO_2F, a commercial V_2O_5, and the earlier reported Li_2VO_2F was then performed to disclose the difference in the load curves, deliverable capacity, intercalation voltage, voltage hysteresis and coulombic efficiency.

2. Experimental

VO_2F powders were synthesized by a simple ball-milling process (WC milling jar with volume of 80 mL, and balls with diameter of 10 mm, 450 rpm for 24 h) using commercial VOF_3 (99%, Sigma-Aldrich) and V_2O_5 (≥99.6%, Sigma-Aldrich) (1 : 1, molar ratio) as precursors. Precursors were added into the WC jar in an argon-filled glovebox. After ball-milling, the powders were collected and stored in a glovebox. The as-milled VO_2F was used as electrode materials without further treatment.

Synchrotron X-ray diffraction (SXRD) patterns were collected at Petra-III beamline P02.1 ($\lambda = 0.2076$ Å) at DESY in Hamburg, Germany. Powders were sealed into 0.5 mm glass capillaries in an argon-filled glovebox. Rietveld structure refinements were performed using FullProf program.[40]

Powder neutron diffraction (ND) experiments were carried out at the CANAM (Center of Accelerators and Nuclear Analytical Methods, LM2011019) infrastructure, Czech Republic. The powder sample of about 1 g was sealed in cylindrical vanadium container with a diameter of 6 mm. The primary neutron beam was monochromatized by a copper mosaic monochromator (reflection 220) providing a neutron beam wavelength of $\lambda =$ 1.46 Å. ND patterns were collected in the 2θ range from 4 to 144° with step of 0.08° and with total time for one diffraction pattern of about 18 h.

Solid-state ^{19}F and ^{51}V magic angle spinning (MAS) nuclear magnetic resonance (NMR) experiments were carried out at resonance frequencies of 338.4 and 94.5 MHz, respectively, on a Bruker Avance spectrometer with a 1.8 mm MAS probe (40 kHz). Experiments were carried out at room temperature with 90°/180°-pulses of 0.8/1.6 μs at 190 W for ^{19}F, and pulse durations of 2.25 μs at 260 W for ^{51}V. ^{19}F and ^{51}V spectra were referenced to $CFCl_3$ (0 ppm) and V_2O_5 powder (0 ppm), respectively.

A slurry consisting of as-milled VO_2F (72 wt%), carbon black (18 wt%) and poly(vinylidene fluoride) (10 wt%) in dimethylformamide was coated onto a stainless steel current collector. The electrodes were dried at 100 °C under vacuum. VO_2F/Li Swagelok cells were assembled using Li foil anode, 1 M $LiPF_6$ in ethylene carbonate/dimethyl carbonate (EC/DMC, 1 : 1 v/v) as electrolyte and two discs of glass fiber as separator in an Ar-filled glovebox. Galvanostatic charge/discharge was carried out between 4.1 and 1.3 V at 25 °C and 50 mA g^{-1}.

For *ex situ* structural analysis of the cycled samples, VO_2F and carbon black composite was used as working electrode without binders. Electrodes were collected and washed using DMC, and then dried at room temperature in an Ar-filled glovebox.

The *in situ* V K-edge X-ray absorption near-edge structure (XANES) spectra were collected at beamline KMC-2 at Bessy II, Berlin, in transmission mode. A home-made cell consisting of two Al plates with rectangular apertures in the center and two sheets of Kapton windows glued on both sides was used.[41] The slurry containing 70 wt% active material, 20 wt% carbon black, and 10 wt% poly(vinylidene fluoride) in dimethylformamide was cast onto a carbon-coated Al foil and dried overnight. The loading of active material on the Al foil was about 5.5 mg cm^{-2}. Li foil was used as counter electrode. 1 M $LiPF_6$ in EC/DMC (1 : 1, v/v) was used as electrolyte. A porous Celgard film was soaked in the electrolyte and used as separator. The cell was placed between two ionization chambers and cycled between 4.1 and 1.3 V *versus* lithium at a current rate of 52 mA g^{-1}, and then at 113 mA g^{-1} at room temperature. The spectra were recorded every 10 to 15 min during one discharge/charge cycle over about 12 h. All spectra were background corrected and normalized with the Athena software package.[42]

3. Results and discussion

3.1. Synthesis and structure of pristine material

Stoichiometric amounts of commercial V_2O_5 and VOF_3 were used as a starting mixture to obtain the target compound VO_2F through the following one-step mechanochemical reaction in a closed milling jar:

$$V_2O_5 + VOF_3 \rightarrow 3VO_2F \quad (2)$$

Formation of VO_2F product was identified by recording its SXRD pattern (Fig. 1). After the mechanochemical ball-milling reaction, all V_2O_5 and VOF_3 precursors have converted into new phase without any further thermal processing. Rietveld refinement of the diffraction pattern was performed using a starting crystal structure model reported by Pérez-Flores *et al.*[39] Refinement with the space group $R\bar{3}c$ (no. 167) gave a good fit to the experimental data. Such phase assumption is also supported by the characteristic splitting of 104 and 110 peaks and the presence of 113 reflection.[43] No impurities can be

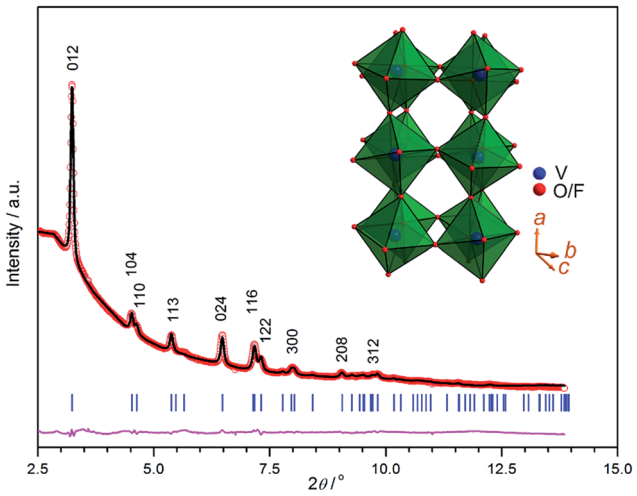

Fig. 1 SXRD pattern and Rietveld refinement for the pristine VO_2F. Bragg peak positions (blue vertical bars) corresponding to the rhombohedral $R\bar{3}c$ cell are given below the pattern. The reliability parameters are: $R_p = 21.8$, $R_{wp} = 13.6$ and $R_{exp} = 43.5$. Inset shows the linkage manner of the corner-shared octahedra in $R\bar{3}c$ phase.

detected for the as-milled powders. Pristine VO_2F crystallizes with a rhombohedral symmetry (VF_3-type crystal structure), consisting of tilted corner-shared $V(O/F)_6$ octahedra, as depicted in the inset of Fig. 1. It has been observed that such structure with flexible corner-connected octahedral network has large structural tunability through tilting and octahedral rotation.[44] The refined cell parameters and average crystallite size of pristine VO_2F are summarized in Table 1. The c/a value of the ball-milled nanosized VO_2F (2.5383) is slightly smaller than that (2.5512) for a high temperature and high pressure (800 °C and 4 GPa) synthesized microsized VO_2F material (about 1 to 60 μm).[39] O and F share the Wyckoff 18e sites with nominal site occupancy of 2/3 and 1/3, respectively. Nevertheless, it cannot be refined accurately based on the X-ray diffraction data due to the near identical scattering properties of O and F. The O/F atomic coordinates are refined to be (0.4212(6), 0, 0.25). The isotropic thermal displacement parameters (U_{iso}) for V and O/F sites are 0.037(5) and 0.029(7), respectively. The calculated material density is 3.408 g cm^{-3}, which is close to that for an isostructural VF_3 (3.363 g cm^{-3}).[45]

Fig. 2 shows solid state ^{51}V and ^{19}F MAS NMR spectra for the as-milled VO_2F and the starting precursors. The NMR chemical shifts are sensitive to components of chemical shielding and quadrupole tensor, as a consequence of a change in crystallographic structure. A single sharp ^{51}V resonance line at 0 ppm was

Table 1 Lattice parameters of the pristine and cycled VO_2F

Samples	As-prepared	1st charge	2nd discharge
Space group	$R\bar{3}c$	$Fm\bar{3}m$	$Fm\bar{3}m$
Lattice constant/Å	$a = 5.1374(4)$ $c = 13.0405(2)$	$a = 4.0932(6)$	$a = 4.1110(8)$
Lattice volume/$Å^3$	298.07	68.58	69.48
Crystallite size/nm	34	3	4

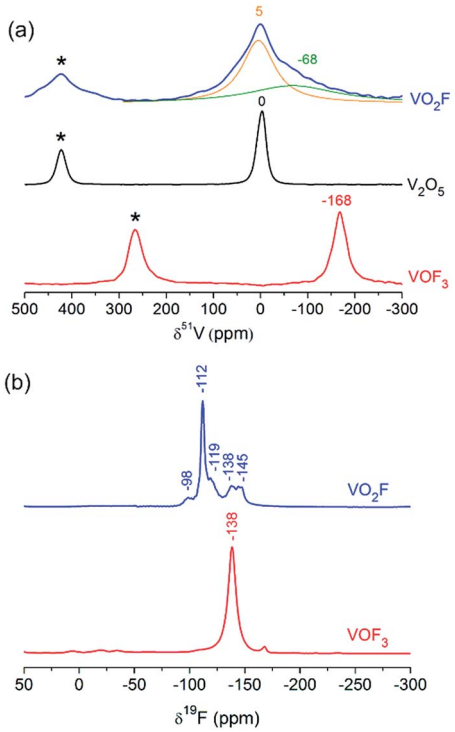

Fig. 2 (a) ^{51}V and (b) ^{19}F MAS NMR for the as-milled VO_2F and starting precursors V_2O_5, VOF_3. The asterisks denote the spinning sidebands.

observed for V_2O_5 and a single resonance line at −168 ppm was observed for VOF_3. In contrast, VO_2F shows a ^{51}V resonance line at 5 ppm (fwhm 83 ppm) with a broad shoulder at −68 ppm (fwhm 230 ppm) (Fig. 2a), indicating the change in the local bonding environments surrounding vanadium. Such observations are in agree with the formation of a new phase, as detected by diffraction experiments. Meanwhile, large difference in the ^{19}F NMR was observed for VO_2F and VOF_3 (Fig. 2b). VOF_3 has one single sharp ^{19}F resonance line at −138 ppm, whereas VO_2F has multiple ^{19}F resonance lines with the strongest one at −112 ppm. The ^{51}V resonance line at 5 ppm and the ^{19}F line at −138 ppm for VO_2F sample may suggest that certain unreacted residuals exist in the final product after ball-milling. These residuals may exist as amorphous state, which are not detectable by diffraction methods. The presence of several weak ^{19}F resonance lines at −98, −119 and −145 ppm may arise from local structure distortion (such as short-range O/F ordering)[46] or unidentified species.

Fig. 3 shows the V K-edge XANES spectra for the as-milled VO_2F and the starting materials V_2O_5 and VOF_3. The similarity in the absorption edges with strong pre-edge peaks at about 5469 eV indicates that V exist mainly as V^{5+} in the as-milled VO_2F. Owing to the high oxidation state of V and an open framework crystal structure, the nanosized VO_2F is considered to be able to store more lithium ions without metal–O/F bond cleavage, as other vanadium-based oxides and vanadates.[47–49]

3.2. Electrochemical properties

Deep lithiation of VO_2F with the attempt to approach the theoretical capacity, as expected in eqn (1), has never been

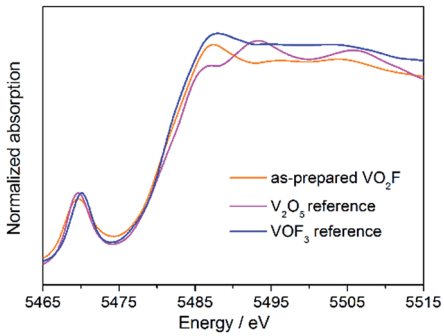

Fig. 3 V K-edge XANES for the as-milled VO_2F and starting precursors V_2O_5, VOF_3.

studied and understood before. The electrochemical properties were evaluated using a VO_2F/Li Swagelok cell. Fig. 4a shows the first three discharge/charge voltage profiles measured at 25 °C and 50 mA g^{-1}. VO_2F was first discharged from its open-circuit voltage (OCV, 3.7 V) to 1.3 V, which shows a lithiation capacity of about 460 mA h g^{-1}, corresponding to 1.75 Li^+ intercalation per formula unit. Several plateau-like voltage steps located at 3.5, 2.8 and 1.7 V were observed, suggesting a continuous structural change upon lithiation, as observed typically for a crystalline orthorhombic V_2O_5 (Fig. 4b). These voltage steps were further highlighted in the dQ/dV curve in Fig. 4c.

Afterwards, the cell was recharged to 4.1 V, which exhibits a sloping charge profile and a charge capacity of about 370 mA h g^{-1}. This indicates that certain amounts of lithium ions were trapped after first discharge. Li trapping inside crystalline V_2O_5 has been also observed due to phase transition.[21] It is estimated that the cycled Li_xVO_2F has a composition of about $x = 0.34$ after first discharge/recharge cycle. Further cycling of the $Li_{0.34}VO_2F$ between 1.3 and 4.1 V leads to steady sloping voltage profiles (Fig. 4a) and high coulombic efficiencies (99.3%, Fig. 4d). The sloping cycling curves indicate a single phase solid solution reaction. The second discharge capacity is about 350 mA h g^{-1}, suggesting a solid solution range between $Li_{0.34}VO_2F$ and $Li_{1.67}VO_2F$, assuming that no side reactions occur. Thus, the ball-milling synthesized nanosized VO_2F shows significant gains in the deliverable capacity over cycling between 4.1 and 1.3 V, compared to the microsized particles.[39] After 50 cycles, the capacity decays to about 215 mA h g^{-1} (Fig. 4d). The capacity decay of VO_2F over 50 cycles is 0.7% per cycle. This is superior to that for V_2O_5 nanoparticles (3.2% decay per cycle over 20 cycles),[50] and close to that for V_2O_5 nanowires supported on graphene (0.6% decay per cycle over 50 cycles)[51] cycled between 4 and 1.5 V.

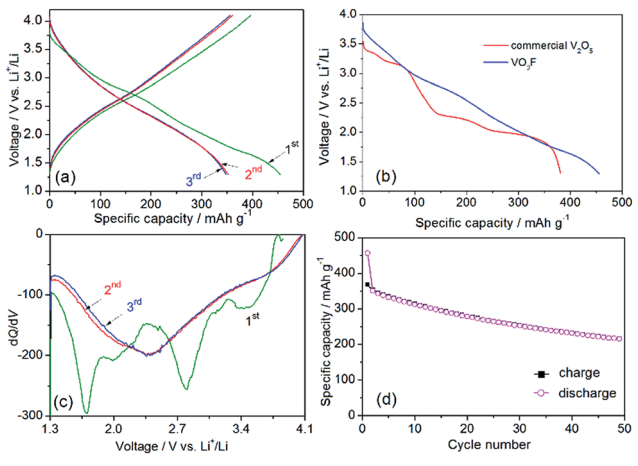

Fig. 4 (a) Galvanostatic discharge/charge voltage profiles (first three cycles) of VO_2F using Li as negative electrode at 25 °C and 50 mA g^{-1}, (b) comparison of the first discharge curves between VO_2F and a commercial V_2O_5 (25 °C, 20 mA g^{-1}), (c) dQ/dV curves, and (d) cycling stability.

The first discharge curve is different from the subsequent charge/discharge curves, indicating that lithium storage proceeds through a different mechanism after the first discharge. Similar voltage profile changes upon lithiation have been previously observed for other materials such as cubic $TiOF_2$,[52] rhombohedral Li_2MoO_4,[12] orthorhombic V_2O_5 (ref. 10) and monoclinic $LiVO_3$ (ref. 53) with discharge voltages centered at 1.2 V (Ti^{4+}/Ti^{2+}), 2.1 V (Mo^{6+}/Mo^{5+}), 2.5 V ($V^{5+}/V^{3.5+}$) and 2.3 V (V^{5+}/V^{4+}), respectively. Most of these materials evolve into a disordered rock-salt phase after one step lithiation. The same behavior is thus expected for the lithiation of VO_2F.

3.3. Structural transition into disordered rock-salt phase

After cycling, clear structural changes were observed from the SXRD patterns. Several broad diffraction peaks located at 2θ of 5.76°, 8.16° and 9.98° for the cycled VO_2F were observed (Fig. 5), revealing that VO_2F transfers to a new phase. Moreover, the diffraction peaks are located at lower d-values for the first charge sample, compared to that for the second discharge sample, which is reasonable due to intercalation of lithium. This suggests the formation of a stable intercalation phase. All diffraction peaks can be well indexed to a cubic cell $Fm\bar{3}m$, as labeled by Miller indices in Fig. 5. The refined lattice constants are summarized in Table 1. The cubic lattice volume expands slightly from the first charge (a = 4.0932 Å) to the second

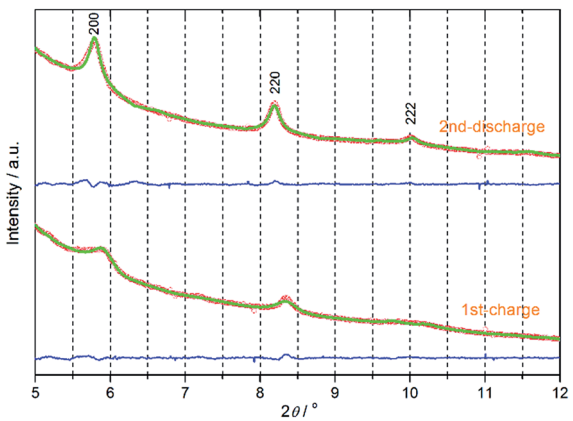

Fig. 5 SXRD patterns and Rietveld refinement using space group $Fm\bar{3}m$ for the 1st charge and 2nd discharge VO_2F samples. Difference plots are shown in blue below the patterns.

discharge (a = 4.1110 Å). For the first charged sample, the diffraction peaks are rather broad and weak. In addition, the refined crystallite size for the cycled samples decreases to about 3 nm (Table 1).

Fig. 6a shows the d-spacing patterns for the cycled samples from combined SXRD and ND diffraction. For the second discharged sample, several diffraction peaks with d-spacings of 2.38 Å (111 diffraction peak) and 1.24 Å (311 diffraction peak) were exclusively observed from the ND diffraction. Other diffraction peaks (200, 220 and 222) can be well resolved from both ND and SXRD.[20,27] Complementary diffraction data from XRD and ND confirm that the cycled VO_2F (Li_xVO_2F) crystallizes in a disorder rock-salt structure (Fig. 6b). Such phase transition occurs during the first lithiation step. Several intermediate phases are likely to form with progressive lithiation and need to be further identified in the future.

It is well-known that deep lithiation of V_2O_5 (below about 1.9 V) leads to an irreversible structural transition into disordered rock-salt ω-$Li_3V_2O_5$ phase.[10] For comparison, Fig. 7 shows the voltage load curves from the second cycles for VO_2F, a commercial orthorhombic V_2O_5 and a previously reported Li_2VO_2F.[20] All three materials show sloping voltage profiles from the second cycles, due to the formation of a similar disordered rock-salt crystal structure. VO_2F with mixed O/F anions show high onset discharge voltage (4.1 V) compared to V_2O_5 (3.7 V). It is reasonable that mixed O/F anionic sublattice favors high intercalation voltage. The redox reactions of V_2O_5 occur in a narrower voltage range between 3.7 and 1.6 V, compared to that for VO_2F and Li_2VO_2F.[20] In addition, V_2O_5 shows the largest voltage hysteresis and the lowest coulombic efficiency (89.5%).

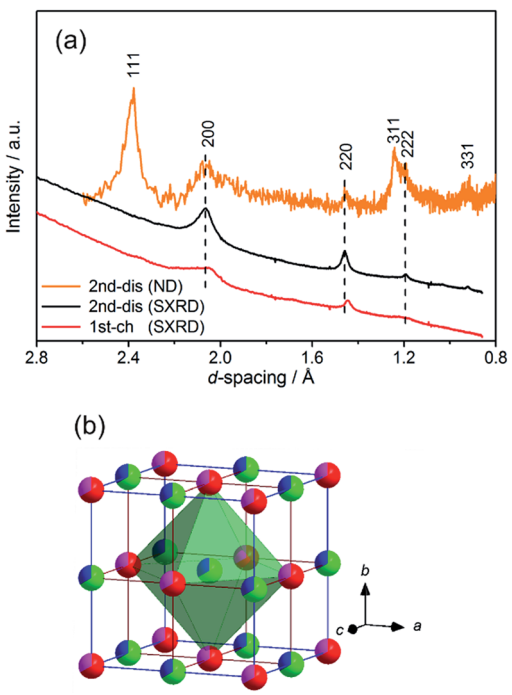

Fig. 6 (a) d-Spacing values from SXRD and ND diffraction of the cycled VO_2F. (b) Disordered rock-salt unit cell.

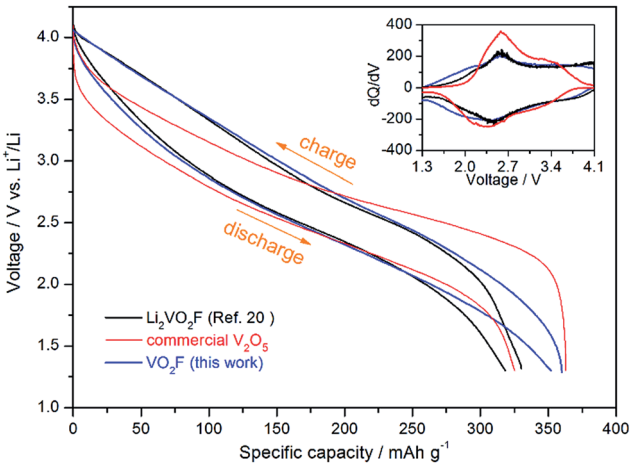

Fig. 7 Voltage load curves at 25 °C from the second cycles for the rhombohedral VO_2F (50 mA g^{-1}), in comparison with that for a previously reported Li_2VO_2F (23 mA g^{-1})[20] and a commercial orthorhombic V_2O_5 (20 mA g^{-1}). Inset shows the corresponding dQ/dV plots.

The load curves for VO_2F and Li_2VO_2F are well overlapped except for the low voltage regions. VO_2F exhibits gentle charge/discharge slope below about 2.2 V, compared to Li_2VO_2F. Accordingly, VO_2F shows a slightly higher capacity of about 30 mA h g^{-1} at the low voltage regions (as also observed in the dQ/dV plots in the inset of Fig. 7), although cycling at slightly higher current density (50 mA g^{-1}), compared to that for Li_2VO_2F (23 mA g^{-1}). Such difference may arise from the different crystallite sizes of both materials, which is about 10 nm for Li_2VO_2F and about 3 nm for newly formed disordered rock-salt VO_2F nanophase. The ultrafine nanoparticles have an enlarged accessible surface area for Li^+ ions. It is considered that the increased capacity at low voltage may arise from an enhanced intercalation process.[20,54] Moreover, based on the calculated composition of $Li_{1.67}VO_2F$ at the end of the second discharge, it is considered that further lithium intercalation (with $x > 1.67$) into disordered rock-salt lattice (with about 16% cation sites unoccupied) may occur at lower discharge cutoff voltages (below 1.3 V).

3.4. *In situ* V K-edge XANES

Changes in electronic structures for VO_2F over galvanostatic cycling were examined by recording the V K-edge XANES spectra during an *in situ* discharge/charge experiment for a VO_2F/Li cell (Fig. 8a). On discharge (from stage OCV to stage E), the main edge shifts to lower energy region by about 3 eV (Fig. 8b). Meanwhile, the intensity of the pre-edge peak decreases and the peak also shifts slightly to lower energy region. This confirms the reduction of vanadium upon lithiation. Based on the observed capacity (1.32 Li^+ capacity), it is considered that the pristine V^{5+} ions are reduced to an average oxidation state of $V^{3.68+}$. The spectral evolution from stage E to stage I is largely reversible upon recharge to 4.1 V. After recharge to 4.1 V, the main edge shifts back to higher energy region, together with increase in the intensity of the pre-edge peak (Fig. 8c). This

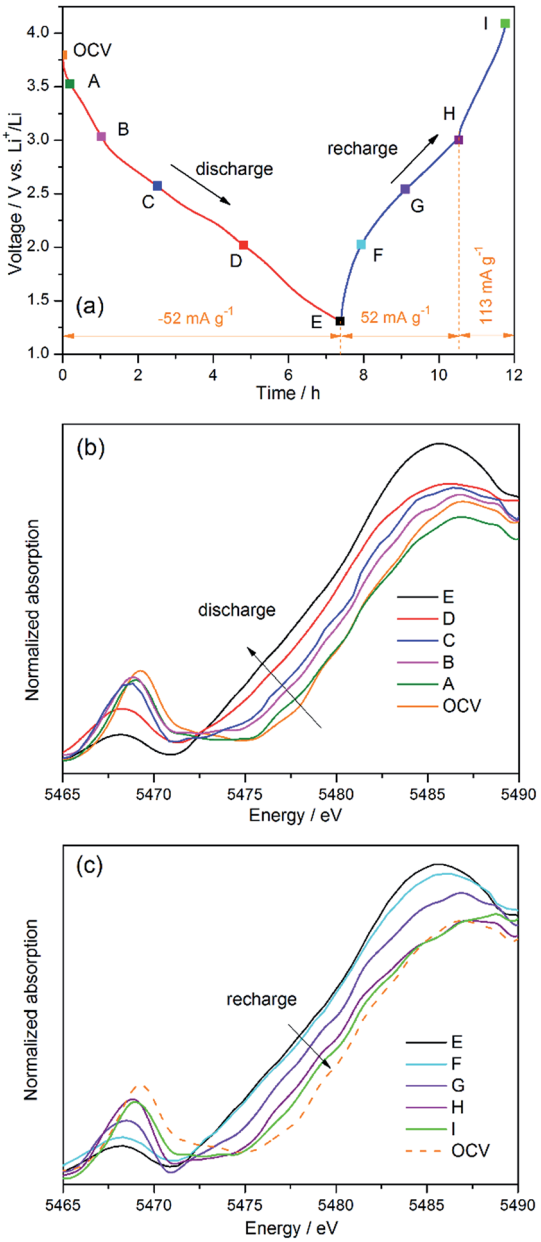

Fig. 8 (a) *In situ* discharge/recharge of a VO_2F/Li cell for collecting V K-edge XANES spectra at room temperature and 52 mA g^{-1}. Higher current (113 mA g^{-1}) was applied in the end of recharge due to refilling of the synchrotron storage ring. Evolution of V K-edge XANES spectra of VO_2F/Li cell during (b) first discharge and (c) recharge.

suggests that recovery of the V oxidation state near V^{5+}. However, the spectrum after recharge is not well overlapped with that of the pristine sample, implying a change in electronic structure due to phase transition.

4. Conclusions

In summary, VO_2F powders have been synthesized through ball-milling V_2O_5 and VOF_3 and have been explored as new high capacity/energy density (theoretically 526 mA h g^{-1} and 1315 W h kg^{-1}) cathode material for rechargeable Li-batteries. First lithiation down to 1.3 V leads to an irreversible phase transition from rhombohedral into a new active disordered rock-salt nanophase, as confirmed by SXRD and ND. Such new phase contributes a high reversible Li^+ intercalation capacity of about 350 mA h g^{-1} at 2.5 V (*i.e.*, 875 W h kg^{-1}). The voltage/structure changes of VO_2F were compared with that for a commercial V_2O_5 and a previously reported Li_2VO_2F. From the second charge/discharge cycles, similar sloping voltage profiles were observed for these materials with disordered rock-salt crystal structure. Compared to V_2O_5, VO_2F shows higher discharge voltage, lower voltage hysteresis and higher coulombic efficiency. In comparison with Li_2VO_2F, a slight extension of the deliverable capacity was observed for VO_2F owing to its ultrafine particle size. Such insights into structural mechanisms may guide the design of other related materials for battery applications. Further investigations need to be carried out to improve the cycling stability and rate performance through controlling the nanoarchitectures, as often strategically used for V_2O_5 and other metal oxides.[55,56]

Acknowledgements

We acknowledge the allocated beamtime at Petra-III (P02.1 beamline, DESY, Hamburg, Germany), Bessy II (KMC-2 beamline, Berlin, Germany), and at the CANAM infrastructure (Ministry of Education, Youth and Sports of the Czech Republic, project: LM2011019, NMI3-II, grant no. 283883).

References

1 M. S. Whittingham, *Chem. Rev.*, 2014, **114**, 11414.
2 K. Mizushima, P. C. Jones, P. J. Wiesman and J. B. Goodenough, *Mater. Res. Bull.*, 1980, **15**, 783.
3 A. K. Padhi, K. S. Nanjundaswamy and J. B. Goodenough, *J. Electrochem. Soc.*, 1997, **144**, 1188.
4 K. Kang, Y. S. Meng, J. Bréger, C. P. Grey and G. Ceder, *Science*, 2006, **311**, 977.
5 A. R. Armstrong and P. G. Bruce, *Nature*, 1996, **381**, 499.
6 M. S. Whittingham, *Chem. Rev.*, 2004, **104**, 4271.
7 G. S. Gautam, P. Canepa, A. Abdellahi, A. Urban, R. Malik and G. Ceder, *Chem. Mater.*, 2015, **27**, 3733.
8 P. Novák and J. Desilvestro, *J. Electrochem. Soc.*, 1993, **140**, 140.
9 N. Jayaprakash, S. K. Das and L. A. Archer, *Chem. Commun.*, 2011, **47**, 12610.
10 C. Delmas, H. Cognac-Auradou, J. M. Cocciantelli, M. Ménétrier and J. P. Doumerc, *Solid State Ionics*, 1994, **69**, 257.
11 C. Delmas, S. Brèthes and M. Ménétrier, *J. Power Sources*, 1991, **34**, 113.
12 D. Mikhailova, A. Voss, S. Oswald, A. A. Tsirlin, M. Schmidt, A. Senyshyn, J. Eckert and H. Ehrenberg, *Chem. Mater.*, 2015, **27**, 4485.
13 V. Pralong, V. Gopal, V. Caignaert, V. Duffort and B. Raveau, *Chem. Mater.*, 2012, **24**, 12.
14 J. Lee, A. Urban, X. Li, D. Su, G. Hautier and G. Ceder, *Science*, 2014, **343**, 519.

15 K. M. Wiaderek, O. J. Borkiewicz, E. Castillo-Martínez, R. Robert, N. Pereira, G. G. Amatucci, C. P. Grey, P. J. Chupas and K. W. Chapman, *J. Am. Chem. Soc.*, 2013, **135**, 4070.
16 J. Zheng, P. Xu, M. Gu, J. Xiao, N. D. Browning, P. Yan, C. Wang and J.-G. Zhang, *Chem. Mater.*, 2015, **27**, 1381.
17 R. Chen, M. Knapp, M. Yavuz, R. Heinzmann, D. Wang, S. Ren, V. Trouillet, S. Lebedkin, S. Doyle, H. Hahn, H. Ehrenberg and S. Indris, *J. Phys. Chem. C*, 2014, **118**, 12608.
18 A. Urban, J. Lee and G. Ceder, *Adv. Energy Mater.*, 2014, **4**, 1400478.
19 N. Yabuuchi, M. Takeuchi, M. Nakayama, H. Shiiba, M. Ogawa, K. Nakayama, T. Ohta, D. Endo, T. Ozaki, T. Inamasu, K. Sato and S. Komaba, *Proc. Natl. Acad. Sci. U. S. A.*, 2015, **112**, 7650.
20 R. Chen, S. Ren, M. Knapp, D. Wang, R. Witter, M. Fichtner and H. Hahn, *Adv. Energy Mater.*, 2015, **5**, 1401814.
21 O. B. Chae, J. Kim, I. Park, H. Jeong, J. H. Ku, J. H. Ryu, K. Kang and S. M. Oh, *Chem. Mater.*, 2014, **26**, 5874.
22 S. Afyon, F. Krumeich, C. Mensing, A. Borgschulte and R. Nesper, *Sci. Rep.*, 2014, **4**, 7113.
23 Q. Liu, Z.-F. Li, Y. Liu, H. Zhang, Y. Ren, C.-J. Sun, W. Lu, Y. Zhou, L. Stanciu, E. A. Stach and J. Xie, *Nat. Commun.*, 2015, **6**, 6127.
24 M. Sathiya, A. S. Prakash, K. Ramesha, J.-M. Tarascon and A. K. Shukla, *J. Am. Chem. Soc.*, 2011, **133**, 16291.
25 Y. Wang, K. Takahashi, K. Lee and G. Z. Cao, *Adv. Funct. Mater.*, 2006, **16**, 1133.
26 V. Petkov, P. N. Trikalitis, E. S. Bozin, S. J. L. Billinge, T. Vogt and M. G. Kanatzidis, *J. Am. Chem. Soc.*, 2002, **124**, 10157.
27 S. Ren, R. Chen, E. Maawad, O. Dolotko, A. A. Guda, V. Shapovalov, D. Wang, H. Hahn and M. Fichtner, *Adv. Sci.*, 2015, **2**, 1500128.
28 N. Recham, J.-N. Chotard, L. Dupont, C. Delacourt, W. Walker, M. Armand and J.-M. Tarascon, *Nat. Mater.*, 2010, **9**, 68.
29 N. Pereira, F. Badway, M. Wartelsky, S. Gunn and G. G. Amatucci, *J. Electrochem. Soc.*, 2009, **156**, A407.
30 M. Duttine, D. Dambournet, N. Penin, D. Carlier, L. Bourgeois, A. Wattiaux, K. W. Chapman, P. J. Chupas, H. Groult, E. Durand and A. Demourgues, *Chem. Mater.*, 2014, **26**, 4190.
31 J. Barker, M. Y. Saidi and J. L. Swoyer, *J. Electrochem. Soc.*, 2004, **151**, A1670.
32 A. P. Wilkinson, R. E. Josefsberg, L. C. Gallington, C. R. Morelock and C. M. Monaco, *J. Solid State Chem.*, 2014, **213**, 38.
33 A. Demourgues, N. Penin, E. Durand, F. Weill, D. Dambournet, N. Viadere and A. Tressaud, *Chem. Mater.*, 2009, **21**, 1275.
34 M. Leblanc, V. Maisonneuve and A. Tressaud, *Chem. Rev.*, 2015, **115**, 1191.
35 N. Louvain, Z. Karkar, M. El-Ghozzi, P. Bonnet, K. Guérin and P. Willmann, *J. Mater. Chem. A*, 2014, **2**, 15308.
36 S. L. Benjamin, W. Levason and G. Reid, *Chem. Soc. Rev.*, 2013, **42**, 1460.
37 G. A. Senchyk, V. O. Bukhan'ko, A. B. Lysenko, H. Krautscheid, E. B. Rusanov, A. N. Chernega, M. Karbowiak and K. V. Domasevitch, *Inorg. Chem.*, 2012, **51**, 8025.
38 G. A. Kolta, D. W. A. Sharp and J. M. Winfield, *J. Fluorine Chem.*, 1979, **14**, 153.
39 J. C. Pérez-Flores, R. Villamor, D. Ávila-Brande, J. M. Gallardo Amores, E. Morán, A. Kuhn and F. García-Alvarado, *J. Mater. Chem. A*, 2015, **3**, 20508.
40 J. Rodríguez-Carvajal, *Phys. B*, 1993, **192**, 55.
41 R. Chen, R. Heinzmann, S. Mangold, V. S. K. Chakravadhanula, H. Hahn and S. Indris, *J. Phys. Chem. C*, 2013, **117**, 884.
42 B. Ravel and M. Newville, *J. Synchrotron Radiat.*, 2005, **12**, 537.
43 B. Li, D. Wang, Y. Wang, B. Zhu, Z. Gao, Q. Hao, Y. Wang and K. Tang, *Electrochim. Acta*, 2015, **180**, 894.
44 J. M. Rondinelli, S. J. May and J. W. Freeland, *MRS Bull.*, 2012, **37**, 261.
45 D. L. Perry, *Handbook of inorganic compounds*, Taylor & Francis, Boca Raton, FL, 2nd edn, 2011, p. 452.
46 L.-S. Du, A. Samoson, T. Tuherm and C. P. Grey, *Chem. Mater.*, 2000, **12**, 3611.
47 N. A. Chernova, M. Roppolo, A. C. Dillon and M. S. Whittingham, *J. Mater. Chem.*, 2009, **19**, 2526.
48 R. Chen, S. Ren, M. Yavuz, A. A. Guda, V. Shapovalov, R. Witter, M. Fichtner and H. Hahn, *Phys. Chem. Chem. Phys.*, 2015, **17**, 17288.
49 R. Chen, S. Ren, X. Mu, E. Maawad, S. Zander, R. Hempelmann and H. Hahn, *ChemElectroChem*, 2016, **3**, 892.
50 S.-H. Ng, T. J. Patey, R. Büchel, F. Krumeich, J.-Z. Wang, H.-K. Liu, S. E. Pratsinis and P. Novák, *Phys. Chem. Chem. Phys.*, 2009, **11**, 3748.
51 H. Liu and W. Yang, *Energy Environ. Sci.*, 2011, **4**, 4000.
52 M. V. Reddy, S. Madhavi, G. V. Subba Rao and B. V. R. Chowdari, *J. Power Sources*, 2006, **162**, 1312.
53 Z. Huang, L. Cao, L. Chen, Y. Kuang, H. Zhou, C. Fu and Z. Chen, *J. Phys. Chem. C*, 2016, **120**, 3242.
54 R. Chen, M. Knapp, M. Yavuz, S. Ren, R. Witte, R. Heinzmann, H. Hahn, H. Ehrenberg and S. Indris, *Phys. Chem. Chem. Phys.*, 2015, **17**, 1482.
55 B. Yan, X. Li, Z. Bai, Y. Zhao, L. Dong, X. Song, D. Li, C. Langford and X. Sun, *Nano Energy*, 2016, **24**, 32.
56 Y. Zhao, X. Li, B. Yan, D. Xiong, D. Li, S. Lawes and X. Sun, *Adv. Energy Mater.*, 2016, **6**, 1502175.

